

**SHORT COMMUNICATION**

# A Variationally Consistent Hyperstatic Reaction Method for Tunnel Lining Design

Hoang-Giang Bui\*<sup>1</sup> | Jelena Ninić<sup>2</sup> | Ngoc-Anh Do<sup>3</sup> | Daniel Dias<sup>4</sup> | Günther Meschke<sup>1</sup>

<sup>1</sup>Institute for Structural Mechanics, Ruhr University Bochum, Germany

<sup>2</sup>University of Nottingham, United Kingdom

<sup>3</sup>Hanoi University of Mining and Geology, Vietnam

<sup>4</sup>University Grenoble Alpes, France

**Correspondence**

\*Hoang-Giang Bui. Email: giang.bui@rub.de

**Present Address**

IC 6/185, Universitätsstrasse 150, 44801 Bochum

**Summary**

In this technical note, a consistent finite element formulation of the Hyperstatic Reaction Method (HRM) for tunnel linings design is proposed by introducing a variational consistently linearized formulation. It permits to consider a nonlinear interaction between a lining structure and the surrounding ground. Recent advances of the HRM in regard to the consideration of the nonlinear response of the segmented tunnel lining exposed to design loads use an iterative algorithm for solving the nonlinear system of equations. In the proposed Variationally consistent Hyperstatic Reaction Method (VHRM), a distributed nonlinear spring model representing the interaction between the lining and the ground soils is considered in a variationally consistent format. Computing the tangential spring stiffness via consistent linearization, and using Newton-Raphson iteration, requires significantly smaller number of iterations as compared to the original HRM model based on nodal springs. Furthermore, the method is applicable for simulations using solid finite elements (2D and 3D), as well as beam or finite shell elements, respectively.

**KEYWORDS:**

Hyperstatic Reaction Method, Lining Design, FEM, Consistent linearization

## 1 | INTRODUCTION

Shield tunnelling is a flexible method for tunnel construction in a broad range of geological conditions and environments, allowing tunneling in urban areas with minimal impact on the existing infrastructure even for low overburdens. Due to the high degree of automation, this technique has proven to be effective in terms of costs and construction time<sup>1</sup>. A large contribution to the construction efficiency is the common use of pre-cast segmented tunnel structures. They are installed ring-by-ring under the protection of the shield machine during the tunnel construction. Such a tunnel structure provides load-bearing capacity immediately after installation and ensures immediate tunnel stability behind the shield.

Numerical models are commonly preferred for the design of segmented tunnel linings against analytical solutions due to their ability to more accurately consider the complex loading conditions and soil-structure interactions. In usual design practice, structural models of the lining are established, representing the surrounding soil by discrete springs whose stiffness is determined as a function of the properties of the surrounding soil and the radius of the lining shell. The lining can either be considered as a continuous structure, or longitudinal joints can be accounted for as either hinges or rotational springs at the segments ends. One of the most commonly used numerical methods for the prediction of the tunnel lining response is the Hyperstatic Reaction Method (HRM)<sup>2,3,4</sup>. This model is characterized by a large number of “Winkler”-type springs<sup>3</sup> for the representation of the bedding of the structure. The loadings from the earth pressure and groundwater are either applied as design loads<sup>5</sup>, as loads back-calculated from in-situ monitoring<sup>6</sup>, or as loading imported from a large scale computational 3D model of the tunnel advancement process<sup>7</sup>. More details about the HRM are given in Section 2. In the original HRM method, the iterative procedure is employed for the calculation of the nonlinear stiffening of the “Winkler”-type springs. This procedure is explicit and requires several hundred steps to yield robust results. In addition, using a fixed point iteration, the final deformation and stiffness of the nonlinear springs are only an approximation of the true equilibrium of the soils-spring system.

In order to provide a fully consistent numerical solution, an improvement of the HRM is proposed by introducing the Variationally consistent Hyperstatic Reaction Method (VHRM). A variational formulation of the nonlinear spring model for modelling the interaction between the lining and the ground is developed and implemented into the open-source Finite Element (FE) framework KRATOS<sup>8</sup>. The tunnel structure is represented either by finite beam or solid elements. The interaction between the lining structure and the soil is represented by nonlinear spring model, characterized by a hyperbolic spring characteristics. Consistent linearization is employed using the Newton-Raphson method in order to simultaneously compute the spring stiffness and the structural deformation. The VHRM has been verified against the existing HRM and further numerical examples have been computed to demonstrate the computational performance of the developed method. The remainder of this technical note is organized as follows: Section 2 gives a brief overview of the HRM; Section 3 presents the formulation and the finite element implementation of the proposed VHRM. In Section 4.1, the implemented formulation is verified against an existing HRM implementation<sup>9</sup>. A selected numerical application of the VHRM method to tunnel lining analysis is presented in Section 4.3. Finally, Section 6 summarizes the achievements and benefits of the proposed method.

## 2 | HYPERSTATIC REACTION METHOD

The HRM is described in detail in<sup>3,4,9,10</sup>. In the original approach, the lining is represented by beam elements. The beam formulation used for the description of the tunnel structure and the definition of the loading acting on the lining are given in the above references. In the HRM, the soil-structure interaction, i.e. the ground support, is modelled as illustrated in Section 1.

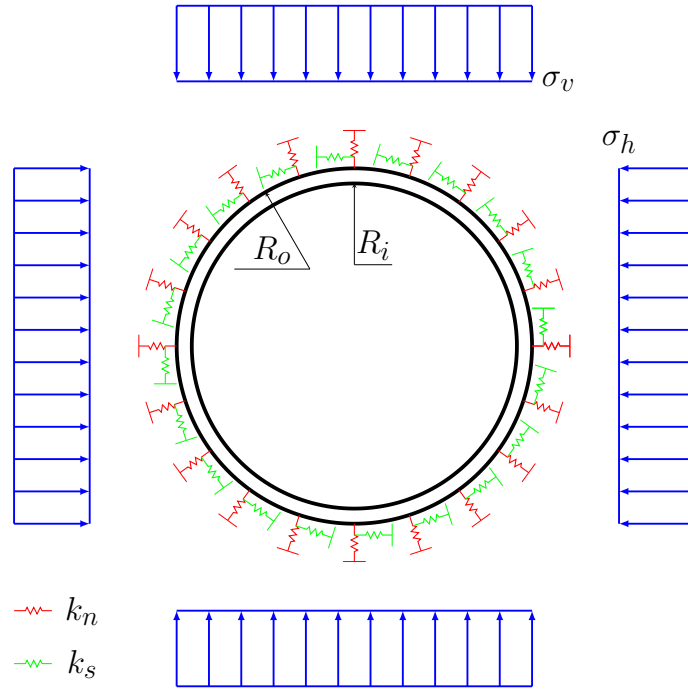


**FIGURE 1** Loading profile and nonlinear springs, representing the soil-structure interaction.

In order to account for the ground support, nonlinear springs are inserted at the nodes of the beams. Both springs in tangential ( $s$ ) and normal ( $n$ ) direction are considered to have a nonlinear stiffness  $\eta_n^*$  and  $\eta_s^*$  as a function of the tangential and normal deformation  $\delta_s$  and  $\delta_n$ , respectively:

$$\begin{aligned}\eta_n^* &= \frac{p_{n,lim}}{\delta_n} \left( 1 - \frac{p_{n,lim}}{p_{n,lim} + \eta_{n,0}\delta_n} \right), \\ \eta_s^* &= \frac{p_{s,lim}}{\delta_s} \left( 1 - \frac{p_{s,lim}}{p_{s,lim} + \eta_{s,0}\delta_s} \right).\end{aligned}\quad (1)$$

$p_{*,lim}$  is the maximum reaction pressure that the soil is able to accommodate, which is computed based on the cohesion  $c$  and friction angle  $\phi$  of the ground:

$$\begin{aligned}p_{n,lim} &= \frac{2c \cos \phi}{1 - \sin \phi} + \frac{1 + \sin \phi}{1 - \sin \phi} \Delta \sigma_{conf}, \\ p_{s,lim} &= \frac{\sigma_h + \sigma_v}{2} \tan \phi.\end{aligned}\quad (2)$$

In Equations (2),  $\sigma_h$  and  $\sigma_v$  are the horizontal and the vertical loads, respectively, acting on the lining. The initial ground stiffness in both normal and tangential direction is defined by:

$$\begin{aligned}\eta_{n,0} &= \beta \frac{1}{1 + \nu_s} \frac{E_s}{R_o}, \\ \eta_{s,0} &= \frac{1}{3} \eta_{n,0}.\end{aligned}\quad (3)$$

where  $\beta$  is an adjustment factor which is typically chosen as  $\beta = 2$ <sup>11</sup>,  $E_s$  denotes the elastic stiffness of the soil and  $R_i, R_o$  is the inner and outer tunnel radius of the tunnel shell, respectively.  $\Delta\sigma_{conf}$  is the confining pressure defined as:

$$\Delta\sigma_{conf} = \frac{\sigma_h + \sigma_v}{2} \frac{\nu_s}{1 - \nu_s}. \quad (4)$$

with  $\nu_s$  as the Poisson's ratio of the soil.

### 3 | VARIATIONALLY CONSISTENT HYPERSTATIC REACTION METHOD

#### 3.1 | Nonlinear spring model for consideration of soil-lining interaction

At each point on the lining-soil interface  $\Gamma_s$ , a local Frénet frame with  $\{\mathbf{n}, \mathbf{s}, \mathbf{t}\}$  as the basis vectors of the local frame is defined. For 2D problem, the tangential vector  $\mathbf{t}$  can be neglected. The spring forces is decomposed into components in this local coordinate system

$$\mathbf{t}^s = r_n \mathbf{n} + r_s \mathbf{s} + r_t \mathbf{t}, \quad (5)$$

with components

$$\begin{aligned} r_n &= \chi p_{n,lim} \ln(p_{n,lim} + \eta_{n,0} \delta_n), \\ r_s &= \chi p_{s,lim} \ln(p_{s,lim} + \eta_{s,0} \delta_s), \\ r_t &= \chi p_{t,lim} \ln(p_{t,lim} + \eta_{t,0} \delta_t). \end{aligned} \quad (6)$$

$\delta_{\square}$  denotes the projection of the displacement  $\mathbf{u}$  onto the local Frénet frame, i.e.  $\delta_n = \langle \mathbf{u} \cdot \mathbf{n} \rangle$ ,  $\delta_s = |\mathbf{u} \cdot \mathbf{s}|$ ,  $\delta_t = |\mathbf{u} \cdot \mathbf{t}|$ , where the function  $\langle x \rangle$  denotes the Macaulay bracket.

The definition of  $\delta_n$  accounts for the fact that the springs are only activated when the lining penetrates into the soil. Unlike  $\delta_n$ , the tangential displacements  $\delta_s$  and  $\delta_t$  are always activated. The definition of  $\delta_s$  and  $\delta_t$  does not take into account the direction of the tangential displacements, leading to a symmetric formulation.

The factor  $\chi$  in Equation (6) is determined by calibrating the traction-displacement relation (6) to the nonlinear spring model according to the HRM model (Section 2). To this end, the stiffness of the nonlinear spring model according to Equation (1) is re-written for the 1D case as

$$\eta^*(\delta) = \frac{p_{lim} \eta_0}{p_{lim} + \eta_0 \delta}. \quad (7)$$

The deformation  $\delta$  caused by a force  $f$  is computed as

$$\delta = \frac{f}{\eta^*(\delta)} = \frac{f p_{lim}}{\eta_0 (p_{lim} - f)}. \quad (8)$$

According to Equation (6), the spring force  $f$  is expressed as a function of the deformation  $\delta$

$$f = \chi p_{lim} \ln(p_{lim} + \eta_0 \delta). \quad (9)$$

From Equation (9) the deformation  $\delta$  can be expressed as

$$\delta = \frac{1}{\eta_0} \left( \exp\left(\frac{f}{\chi p_{lim}}\right) - p_{lim} \right) \quad (10)$$

Combining Equation (8) and (10) allows to determine the load factor  $\chi$  in (6) as:

$$\chi = \frac{f}{p_{lim} \ln\left(\frac{p_{lim}^2}{p_{lim} - f}\right)}. \quad (11)$$

The force  $f$  is assumed as the axial force of the springs, can be taken as the pressure on a point on the lining, which reads:

$$f = \sqrt{\sigma_v^2 + \sigma_h^2} \quad (12)$$

### 3.2 | Virtual work of the springs

The potential energy of the springs has the form

$$W^s = \int_{\Gamma_s} \mathbf{u} \cdot \mathbf{t}^s d\Gamma. \quad (13)$$

The virtual work of the springs is obtained by taking the variation of the potential energy as

$$\delta W^s = \int_{\Gamma_s} \delta (r_n \mathbf{u} \cdot \mathbf{n} + r_s \mathbf{u} \cdot \mathbf{s} + r_t \mathbf{u} \cdot \mathbf{t}) d\Gamma. \quad (14)$$

We have

$$\delta (r_n \mathbf{u} \cdot \mathbf{n} + r_s \mathbf{u} \cdot \mathbf{s} + r_t \mathbf{u} \cdot \mathbf{t}) = \delta r_n \mathbf{u} \cdot \mathbf{n} + \delta r_s \mathbf{u} \cdot \mathbf{s} + \delta r_t \mathbf{u} \cdot \mathbf{t} + \delta \mathbf{u} \cdot \mathbf{t}^s, \quad (15)$$

From Equation (32), we can infer that

$$\delta r_n = k_n \delta \mathbf{u} \cdot \mathbf{n}, \quad \delta r_s = k_s \delta \mathbf{u} \cdot \mathbf{s}, \quad \delta r_t = k_t \delta \mathbf{u} \cdot \mathbf{t}. \quad (16)$$

Inserting Equations (16) (15) into (14), one obtains:

$$\begin{aligned}\delta W^s &= \int_{\Gamma_s} [(\delta \mathbf{u} \otimes \mathbf{u}) : (k_n \mathbf{n} \otimes \mathbf{n} + k_s \mathbf{s} \otimes \mathbf{s} + k_t \mathbf{t} \otimes \mathbf{t}) + \delta \mathbf{u} \cdot \mathbf{t}^s] d\Gamma \\ &= \int_{\Gamma_s} [(\delta \mathbf{u} \otimes \mathbf{u}) : \mathbf{k}^s + \delta \mathbf{u} \cdot \mathbf{t}^s] d\Gamma.\end{aligned}\quad (17)$$

The expression of the virtual work in (17) can be simplified, neglecting the second order term appearing in the complete expression, to become

$$\delta W^s = \int_{\Gamma_s} \delta \mathbf{u} \cdot \mathbf{t}^s d\Gamma. \quad (18)$$

From a practical standpoint, this neither affects the accuracy nor the convergence of the nonlinear solution scheme, providing that a consistent linearization is used.

### 3.3 | Principle of virtual work considering soil-structure interaction

The principle of virtual work governing the present structural mechanics problem reads

$$\delta \mathcal{W}(\mathbf{u}, \delta \mathbf{u}) = \delta \mathcal{W}^{ext}(\delta \mathbf{u}) - \delta \mathcal{W}^i(\mathbf{u}, \delta \mathbf{u}) - \delta \mathcal{W}^s(\mathbf{u}, \delta \mathbf{u}) = 0, \quad (19)$$

where  $\delta \mathcal{W}^i$  and  $\delta \mathcal{W}^{ext}$  are the contributions of the internal and external forces, respectively, and  $\delta \mathcal{W}^s$  considers the contribution of the soil-structure interaction:

$$\delta \mathcal{W}^{ext}(\delta \mathbf{u}) = \int_{\Omega} \delta \mathbf{u} \cdot \mathbf{b} dV + \int_{\Gamma_t} \delta \mathbf{u} \cdot \mathbf{t} d\Gamma \quad (20)$$

$$\delta \mathcal{W}^i(\mathbf{u}, \delta \mathbf{u}) = \int_{\Omega} \delta \boldsymbol{\varepsilon} : \boldsymbol{\sigma} dV, \quad (21)$$

$$\delta \mathcal{W}^s(\mathbf{u}, \delta \mathbf{u}) = \int_{\Gamma_s} \delta \mathbf{u} \cdot \mathbf{t}^s(\mathbf{u}) d\Gamma. \quad (22)$$

In (22),  $\mathbf{b}$  represents the body force and  $\mathbf{t}$  is the traction acting on the Neumann boundary  $\Gamma_t$ .  $\Gamma_d$  is the domain where the Dirichlet boundary condition is applied.  $\mathbf{u} = \mathbf{u}(\mathbf{X})$  represents the displacement at the spatial point  $\mathbf{X}$ .  $\delta \mathbf{u}$  and  $\delta \boldsymbol{\varepsilon}$  are the variations of displacements and strains, respectively. We further assume a small strain approximation, hence  $\boldsymbol{\varepsilon} = \nabla^s \mathbf{u}$  and  $\delta \boldsymbol{\varepsilon} = \nabla^s \delta \mathbf{u}$ . The Cauchy stress tensor  $\boldsymbol{\sigma} = \boldsymbol{\sigma}(\boldsymbol{\varepsilon})$  depends on the strain via an appropriate constitutive model, and the spring force  $\mathbf{t}^s(\mathbf{u})$  represents the interaction between the soil and the lining.  $\Gamma_s$  denotes the interaction domain between the soil and the lining, i.e. the outer surfaces of the lining ring.

It is noted, that, unlike the standard HRM method, which collocates the contribution of the springs at the node, the contribution of the springs is integrated along the surface  $\Gamma^s$  and requires an integration rule on the surface element. Therefore, a surface discretization is required.

### 3.4 | Finite Element discretization

Using the standard Bubnov-Galerkin displacement-based finite element method, the displacement  $\mathbf{u}$  and its variation  $\delta\mathbf{u}$  are discretized as

$$\mathbf{u}^h = \sum_i N_i \bar{\mathbf{u}}_i \quad \delta\mathbf{u}^h = \sum_i N_i \delta\bar{\mathbf{u}}_i, \quad (23)$$

where  $\bar{\mathbf{u}}_i$  and  $\delta\bar{\mathbf{u}}_i$  denote the nodal displacement and its variation, i.e. the virtual displacement, respectively. Correspondingly, the strain  $\boldsymbol{\epsilon}$  is discretized as

$$\boldsymbol{\epsilon}^h = \nabla^s \sum_i N_i \bar{\mathbf{u}}_i = \sum_i (\nabla^s N_i) \bar{\mathbf{u}}_i, \quad (24)$$

with the strain-displacement operator  $\nabla^s N_i$ . In the following, matrix notation is used, replacing (24) by  $\boldsymbol{\epsilon}^h = \mathbf{B}\bar{\mathbf{u}}$

The discretized virtual work leads to the residual forces

$$\mathbf{r}(\mathbf{u}) = \mathbf{r}^{ext} - \mathbf{r}^s - \mathbf{r}^i, \quad (25)$$

with the external forces

$$\mathbf{r}^{ext} = \int_{\Omega} \mathbf{N}\mathbf{b} dV + \int_{\Gamma_t} \mathbf{N}\mathbf{t} d\Gamma, \quad (26)$$

the internal forces

$$\mathbf{r}^i(\mathbf{u}) = \int_{\Omega} \mathbf{B}^T \boldsymbol{\sigma} dV \quad (27)$$

and the spring forces

$$\mathbf{r}^s(\mathbf{u}) = \int_{\Gamma^s} \mathbf{N}\mathbf{t}^s(\mathbf{u}) d\Gamma. \quad (28)$$

Linearization of the internal forces results in the tangent stiffness matrix

$$\mathbf{K}^t = \frac{\partial \mathbf{r}^i(\mathbf{u})}{\partial \mathbf{u}} = \int_{\Omega} \mathbf{B}^T \mathbb{C} \mathbf{B} dV, \quad (29)$$

where  $\mathbb{C}$  is the tangent stiffness matrix, with  $\mathbb{C} = \mathbb{C}^e$  in the case of a linear elastic model. Linearization of the spring forces gives rise to the tangent spring stiffness matrix

$$\mathbf{K}^s = \frac{\partial \mathbf{r}^s(\mathbf{u})}{\partial \mathbf{u}} = \int_{\Gamma^s} \mathbf{N}\mathbf{k}^s(\mathbf{u}) d\Gamma, \quad \mathbf{k}^s = \frac{\partial \mathbf{t}^s(\mathbf{u})}{\partial \mathbf{u}}. \quad (30)$$

### 3.5 | Linearization of the spring forces

The linearization of  $\mathbf{t}^s$  with respect to the displacement  $\mathbf{u}$  yields the tangential spring stiffness as

$$\mathbf{k}^s = \frac{\partial \mathbf{t}^s(\mathbf{u})}{\partial \mathbf{u}} = \mathbf{n} \otimes \frac{\partial r_n}{\partial \mathbf{u}} + \mathbf{s} \otimes \frac{\partial r_s}{\partial \mathbf{u}} + \mathbf{t} \otimes \frac{\partial r_t}{\partial \mathbf{u}}, \quad (31)$$

with the components

$$\begin{aligned} \frac{\partial r_n}{\partial \mathbf{u}} &= k_n \mathbf{n}, \quad k_n = \begin{cases} \frac{\chi p_{n,lim} \eta_{n,0}}{p_{n,lim} + \eta_{n,0} \delta_n} & \text{if } \mathbf{u} \cdot \mathbf{n} \geq 0, \\ 0 & \text{if } \mathbf{u} \cdot \mathbf{n} < 0, \end{cases} \\ \frac{\partial r_s}{\partial \mathbf{u}} &= k_s \mathbf{s}, \quad k_s = \begin{cases} \frac{\chi p_{s,lim} \eta_{s,0}}{p_{s,lim} + \eta_{s,0} \delta_s} & \text{if } \mathbf{u} \cdot \mathbf{s} \geq 0, \\ -\frac{\chi p_{s,lim} \eta_{s,0}}{p_{s,lim} + \eta_{s,0} \delta_s} & \text{if } \mathbf{u} \cdot \mathbf{s} < 0, \end{cases} \\ \frac{\partial r_t}{\partial \mathbf{u}} &= k_t \mathbf{t}, \quad k_t = \begin{cases} \frac{\chi p_{t,lim} \eta_{t,0}}{p_{t,lim} + \eta_{t,0} \delta_t} & \text{if } \mathbf{u} \cdot \mathbf{t} \geq 0, \\ -\frac{\chi p_{t,lim} \eta_{t,0}}{p_{t,lim} + \eta_{t,0} \delta_t} & \text{if } \mathbf{u} \cdot \mathbf{t} < 0. \end{cases} \end{aligned} \quad (32)$$

From Equations (31) (32), the tangential spring stiffness matrix can be written as

$$\mathbf{k}^s = k_n \mathbf{n} \otimes \mathbf{n} + k_s \mathbf{s} \otimes \mathbf{s} + k_t \mathbf{t} \otimes \mathbf{t}. \quad (33)$$

Note that due to the small strain assumption, the local Frénet frame is evaluated in the undeformed configuration. Therefore, it can be computed at the beginning of the calculation step and kept frozen during the Newton-Raphson iteration. Hence, linearization of  $\mathbf{n}$ ,  $\mathbf{s}$  and  $\mathbf{t}$  is not necessary.

## 4 | COMPARATIVE ASSESSMENT OF THE VHRM VERSUS THE HRM

### 4.1 | Deformations, bending moments and normal forces in continuous linings structure

For verification of the VHRM formulation, a continuous lining model using beam elements is analyzed using both the HRM and the VHRM model. The soil parameters used in both simulations are summarized in Table 1.

The tunnel is characterized by radius  $R_0 = 4.7$  m and overburden of 15.3 m. The lining structure is modelled by finite beam elements based on the Bernoulli beam theory with a depth  $B = 2$  m, a thickness  $t = 0.4$  m. The elasticity modulus of the concrete is  $E = 35 \times 10^3$  MPa. According to the loading profile in Figure 1, the vertical loading and horizontal loading are assumed as  $\sigma_v = 0.34$  MPa and  $\sigma_h = K_0 \sigma_v$ , with the lateral earth pressure coefficient chosen as  $K_0 = 0.5$ .



Parameter	Symbol	Value	Unit
Ground modulus	$E_s$	150.0	$MPa$
Poisson ratio	$\nu_s$	0.3	
Ground density	$\rho_s$	17000	$N/m^3$
Cohesion	$c$	5	$kPa$
Friction angle	$\phi$	37	degree

**TABLE 1** Numerical verification: Soil parameters.

The calculation with the classical HRM method is performed using the FEMSL code<sup>12</sup> with 1000 iterations. The tunnel ring is discretized by means of 400 beam elements. The analysis with the VHRM is performed using the same discretization with Bernoulli beams.

Figure 4.1 shows the deformation of the lining (left) and the rotation angle (right) obtained from the HRM and VHRM method, respectively. The vertical displacement of the tunnel lining is obtained as  $\delta_{VHRM} = 6.844$  mm by the VHRM model, and as  $\delta_{HRM} = 6.808$  mm by the HRM model. The difference of both models is  $\sim 0.5\%$ . The slight differences in vertical

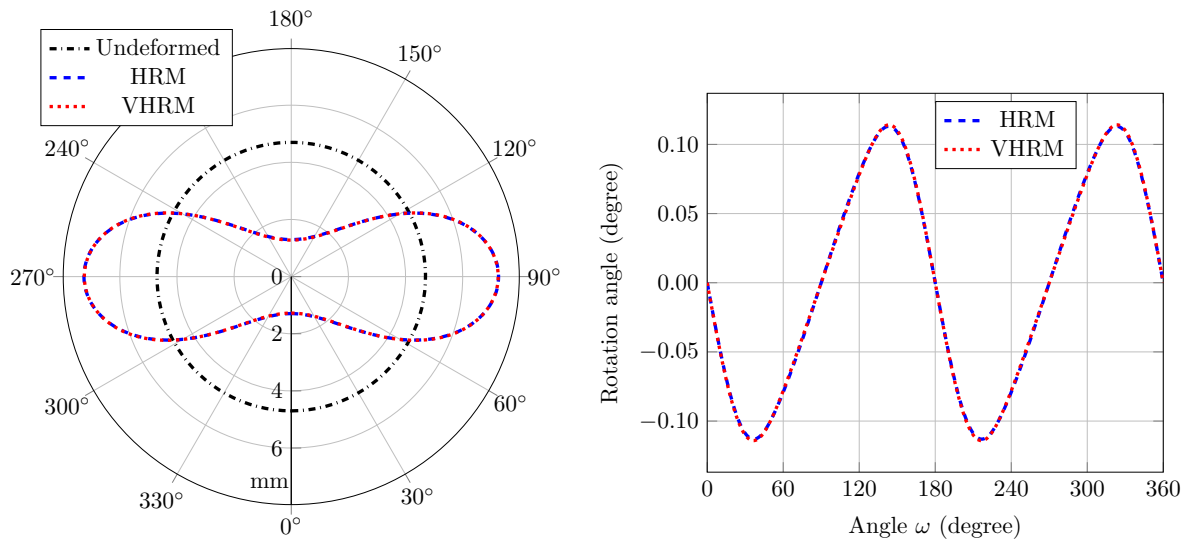


**FIGURE 2** Comparison of the HRM and the VRM model: Left: Deformations of the lining, (magnification factor = 500), right: rotation angles  $\omega$ .

displacements can be explained by the fact, that the displacements in the HRM result from a fixed-point iteration and do not fully satisfy the equilibrium condition.

Figure 3 illustrates the computed bending moment (left) and normal force (right) on the lining using the HRM and the VHRM, respectively. The differences between both models are recorded at  $\omega = 90^\circ$  and  $\omega = 270^\circ$  as  $\sim 0.45\%$  for the moments and  $\sim 4.47\%$  for the normal force.

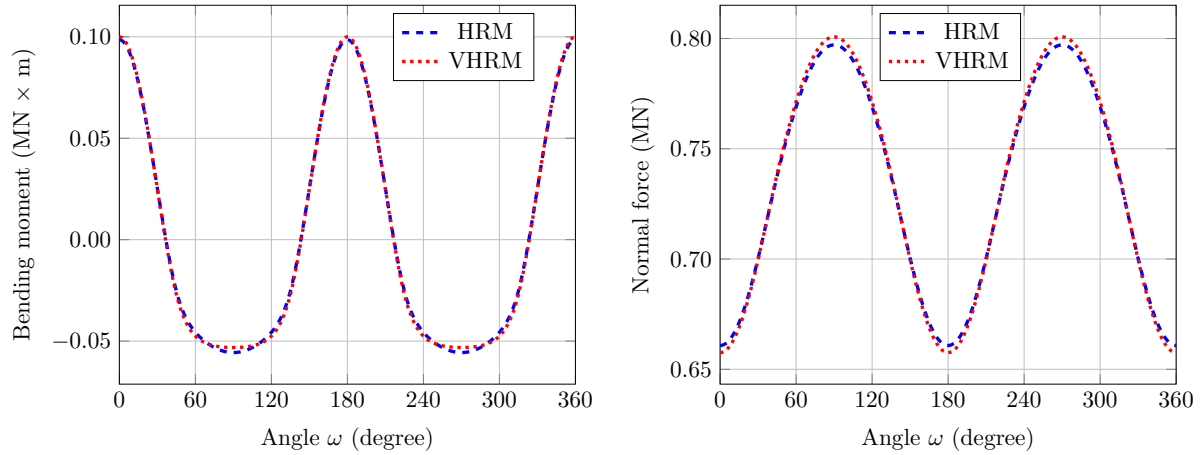


**FIGURE 3** Comparison of the HRM and the VRM model: Bending moment (left) and normal force (right).

## 4.2 | Evaluation of computational efficiency

In this subsection, the computational efficiency of the proposed VHRM model is compared to the original HRM model, using the same continuous lining structure as before. As mentioned in Section 2, the HRM method uses the nonlinear spring model for the soil-structure interaction and employs a fixed-point iteration loop to update the stiffness iteratively. This procedure converges slowly and requires more than 20 iterations to obtain an asymptotically converged vertical displacement (Figure 4).

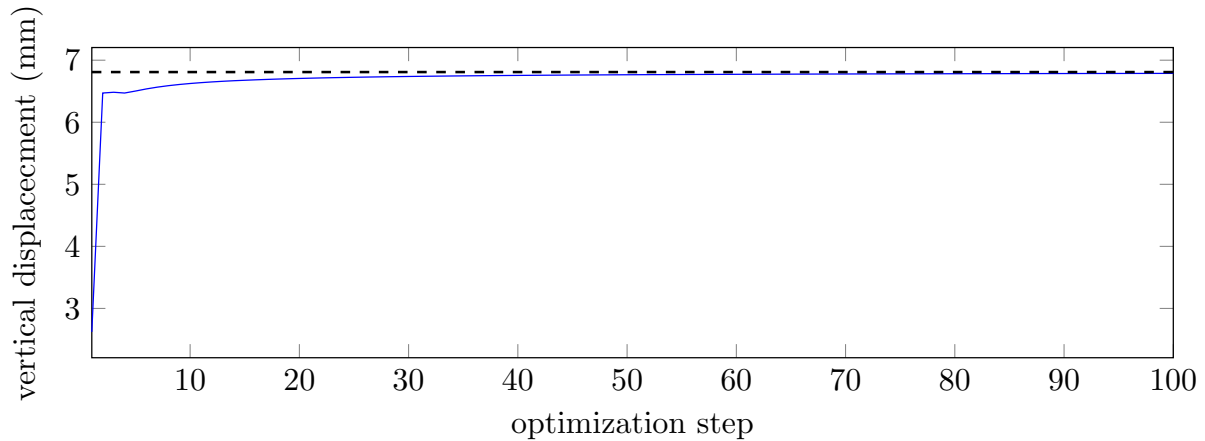


**FIGURE 4** Convergence of vertical displacement using the HRM.

In contrast, the VHRM takes five Newton-Raphson steps to converge to the residual error norm tolerance  $10^{-11}$  (see Table 2). Asymptotic quadratic convergence is observed. In terms of computational time, the iterative procedure used in the HRM takes 4.56 s for 100 steps, whereas the simulation with the VHRM takes only 0.18 s. The computation is performed using one core on a laptop computer with CPU Intel Core-i7 2.4 GHz and 16GB of memory.

Step 1	Step 2	Step 3	Step 4	Step 5
6.779320e-03	5.946327e-04	2.502768e-06	7.246955e-11	6.595405e-12

**TABLE 2** Convergence of the residual norm using the VHRM method.

### 4.3 | Tunnel lining analysis using solid finite elements

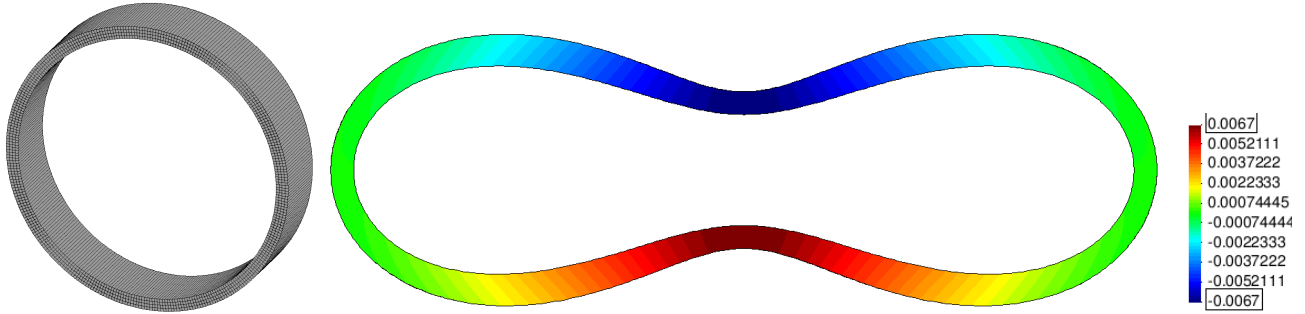


**FIGURE 5** Left: Tunnel shell discretized by solid finite elements. Right: Vertical deformation of the continuous VHRM lining model using solid elements (magnification factor = 500).

In this example, the VHRM is applied to a numerical analysis of a tunnel shell using solid finite elements. In this analysis, the tunnel shell is again idealized as a continuous structure, disregarding joints.

For the present benchmark analysis, 27-node hexahedra elements with Lagrange shape function are used. The mesh is shown in Figure 5 (left) and contains 320 elements along the circumferential direction, 4 elements along the thickness and one element along the longitudinal direction. The parameters of the tunnel lining and the ground are identical to the previous example.

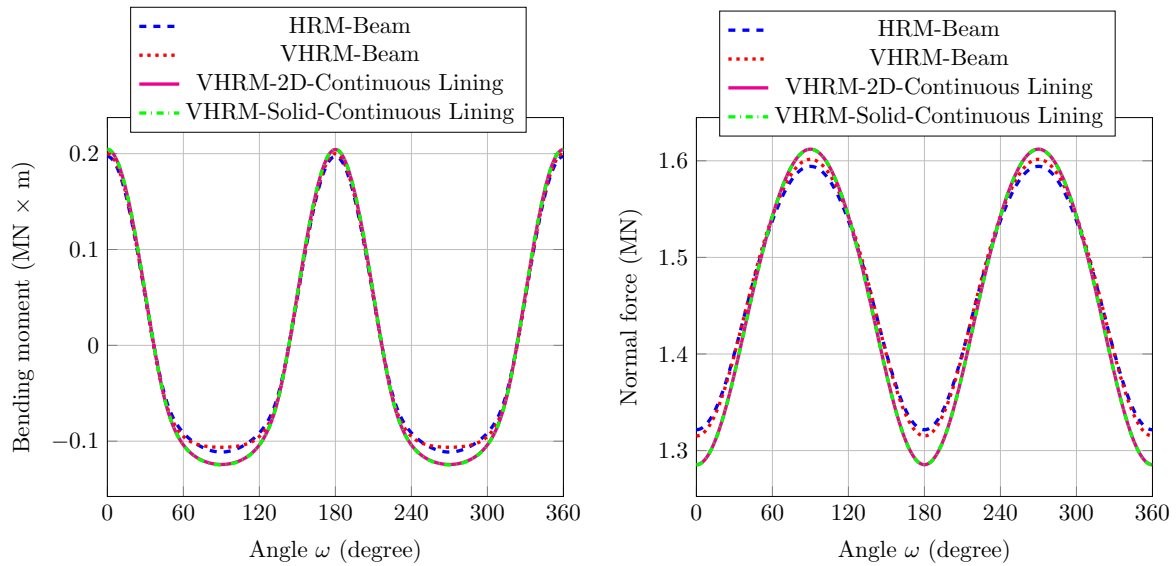
Figure 5 (right) illustrates the deformed configuration of the lining with 500-fold magnification of the displacements. The vertical displacement of the lining is computed as  $\sim 6.65$  mm at the crown position, which is  $\sim 2.4\%$  difference to the displacement computed by the HRM using beam elements.

Figure 6 shows the bending moments and normal forces in the lining. One can see that the VHRM predicts slightly larger bending moments and normal forces than the HRM beam model. A relative difference of 4.3 % and 13.4 % is obtained at the crown for the bending moment and at the side for the normal force, respectively.

Table 3 reports the reduction of the residual VHRM norm. Similar to the VHRM using a finite beam model, only five Newton-Raphson iterations are required to converge to an error norm of  $10^{-11}$ , exhibiting a quadratic rate of convergence.

Step 1	Step 2	Step 3	Step 4	Step 5
1.70908e-03	1.18204e-04	5.99648e-07	1.5031e-11	6.89547e-18

**TABLE 3** Convergence of the residual norm using the VHRM method with solid elements.



**FIGURE 6** Comparison of bending moments (left) and normal forces (right) obtained from the HRM beam model, the VHRM beam model and the VHRM using solid elements.

## 5 | DISCUSSION AND POSSIBLE EXTENSIONS

The VHRM allows to be applied for any finite element discretization of segmental linings, be it beam, shell or solid elements, while the HRM is restricted to beam elements only. This opens a large potential to apply the VHRM for larger tunnel sections and problems that involve complex (curved) tunnel geometries<sup>13</sup>, to analyze the non-linear structural response to earth and groundwater pressure, considering soil-structure interactions, construction induced loadings, and segment-to-segment interaction effects. Moreover, using different interpolation scheme in the context of the finite element method, such as isogeometric analysis, enables further improvements of the efficiency. This opens the possibility to apply this method for integrated design-assessment workflow for the optimization of large tunnel sections in early design stages.

In terms of the nonlinear soil-structure interaction, considering the tunnel in rocks, the VHRM may need to be re-formulated to account for continua containing microstructures. In this regard, the method of virtual power may come in handy since it provides a generalization of the method of virtual work based on the energy principle<sup>14</sup>. Applications in this direction exist<sup>15,16</sup>, where the virtual power principle provides a useful way to avoid the sophisticated mathematical assumption of the segmented joints and allows for the direct input of measured interfacial discontinuities obtaining from the experiment<sup>16</sup>. The assumption of soil-medium in HRM is considered as an isotropic elastic medium. To account for anisotropy, the springs forces have to be improved to include the anisotropic effect. A trivial solution to attain this effect is to introduce different  $\chi$  factors for the normal and tangential springs (see (32)). These factors shall be then calibrated based on soil experimental data.

## 6 | CONCLUSIONS

The HRM method is an effective tool to predict the displacements and the forces, as well as the bending moments in tunnel linings resulting from the soil-structure interaction by employing a simple spring stiffness model. The VHRM method presented in this work extends the HRM by introducing the nonlinear elastic spring stiffness, which substitutes the effect of the bedding of the tunnel lining shell in the ground, directly in the weak form. Hence, in contrast to the HRM, the equilibrium equations and the equations governing the nonlinear spring model are solved concurrently. In the proposed VHRM formulation, a consistent linearization is used along with a standard Newton-Raphson scheme to provide a quadratic convergence of the system solution. In contrast, the implementation of the HRM as was proposed in<sup>9</sup> uses a fixed-point iteration loop to update the spring stiffnesses iteratively. It was shown that the computational efficiency of VHRM significantly exceeds the efficiency of the existing HRM implementations by orders of magnitude, while preserving the accuracy of the solution, as was shown in a verification example. To reproduce the benchmark examples and use the VHRM implementation for lining analysis, a Docker image is created and can be found at [https://hub.docker.com/repository/docker/vrry/kratos\\_bcn2-vhrm\\_paper](https://hub.docker.com/repository/docker/vrry/kratos_bcn2-vhrm_paper).

## Acknowledgements

This presented work was conducted in the framework of Subproject C1 of the Collaborative Research Project SFB 837 "Interaction Modeling in Mechanized Tunneling", financed by the German Research Foundation (DFG) (Grant agreement 77309832). The authors would like to thank the DFG for the support of this project. The second author has received funding for the SAT-BIM project from the European Union's Horizon 2020 research and innovation program under the Marie Skłodowska-Curie grant agreement No. 702874. The second author would like to gratefully acknowledge this support. The third author thanks the support from the Vietnam National Foundation for Science and Technology Development (NAFOSTED) under grant number 105.08-2018.310.

## Author Contributions

Hoang-Giang Bui: study conception, performed the analysis, data interpretation, wrote the paper; Jelena Ninić: writing, reviewing and editing the paper; Ngoc-Anh Do: reviewed the concept and edited the paper; Daniel Dias: reviewed the concept and edited the paper; Günther Meschke: supervision, writing, review and editing.

## References

1. Maidl B, Herrenknecht M, Maidl U, Wehrmeyer G. *Mechanised shield tunnelling*. Ernst und Sohn . 2013.

2. Duddeck H, Erdmann J. On structural design models for tunnels in soft soil. *Underground Space* 1985; 9: 246–259.
3. Oreste P. A numerical approach to the hyperstatic reaction method for the dimensioning of tunnel supports. *Tunnelling and Underground Space Technology* 2007; 22(2): 185–205.
4. Do NA, Dias D, Oreste P, Djeran-Maigre I. 2D numerical investigation of segmental tunnel lining behavior. *Tunnelling and Underground Space Technology* 2013; 37: 115–127.
5. H.Takano Y. Guidelines for the design of shield tunnel lining. *Tunnelling and Underground Space Technology* 2000; 15(3): 303 - 331.
6. Bonini M, Lancellotta G, Barla G. State of stress in tunnel lining in squeezing rock conditions. *Rock Mechanics and Rock Engineering* 2013; 46(2): 405–411.
7. Ninić J, Meschke G. Simulation based evaluation of time-variant loadings acting on tunnel linings during mechanized tunnel construction. *Engineering Structures* 2017; 135: 21–40.
8. Dadvand P, Rossi R, Oñate E. A Framework for Developing Finite Element Codes for Multi-disciplinary Applications. In: Schrefler B, Perego U., eds. *Proceedings of the 8th World Congress on Computational Mechanics* International Center for Numerical Methods in Engineering (CIMNE); 2008; Venice, Italy.
9. Do NA, Dias D, Oreste P, Djeran-Maigre I. A new numerical approach to the hyperstatic reaction method for segmental tunnel linings. *International Journal for Numerical and Analytical Methods in Geomechanics* 2014; 38(15): 1617–1632.
10. Kroetz HM, Do NA, Dias D, Beck AT. Reliability of tunnel lining design using the Hyperstatic Reaction Method. *Tunnelling and Underground Space Technology* 2018; 77: 59–67.
11. Do NA, Dias D, Oreste P, Djeran-Maigre I. The behaviour of the segmental tunnel lining studied by the hyperstatic reaction method. *European Journal of Environmental and Civil Engineering* 2014; 18(4): 489–510.
12. Dias D. FEMSL source. 2016.
13. Ninic J, Bui HG, Meschke G. BIM-to-IGA: A fully automatic design-through-analysis workflow for segmented tunnel linings. *Advanced Engineering Informatics* 2020; 46: 101137.
14. Germain P. The Method of Virtual Power in Continuum Mechanics. Part 2: Microstructure. *SIAM Journal on Applied Mathematics* 1973; 25(3): 556–575.
15. Höller R, Aminbaghai M, Eberhardsteiner L, et al. Rigorous amendment of Vlasov's theory for thin elastic plates on elastic Winkler foundations, based on the Principle of Virtual Power. *European Journal of Mechanics - A/Solids* 2019; 73: 449–482.

16. Zhang JL, Vida C, Yuan Y, Hellmich C, Mang HA, Pichler B. A hybrid analysis method for displacement-monitored segmented circular tunnel rings. *Engineering Structures* 2017; 148(Supplement C): 839 - 856.
17. Ip SCY, Choo J, Borja RI. Impacts of saturation-dependent anisotropy on the shrinkage behavior of clay rocks. *Acta Geotechnica* 2021.

